



Compliant Needle Modeling and Steerable Insertion Simulation

Libo Tang¹, Yonghua Chen² and Xuejian He³

¹The University of Hong Kong, tanglibo@hku.hk

²The University of Hong Kong, yhchen@hku.hk

³The University of Hong Kong, hexuejian@hku.hk

ABSTRACT

Needle based surgery is an important surgical technique for its minimally invasive interventions. The insertion of a long and slender needle into the complicated human body is a very challenging procedure. In this paper, a compliant needle is designed to facilitate the obstacle avoidance and path control that are inevitable in some surgical operations. During needle insertion, a magnetic force is employed to steer the compliant needle when needed. The steerable needle insertion process is simulated in a haptic system which can provide users both visual and haptic feedback.

Keywords: compliant needle, needle insertion, haptic simulation.

DOI: 10.3722/cadaps.2008.39-46

1. INTRODUCTION

Needle or catheter insertion is one of the most common minimally invasive surgery (MIS). It involves inserting long, slender needles or catheters deep into human body for biopsy or drug delivery. For needle/catheter insertion, surgeons often rely on the knowledge of anatomic structures, pre-operative imaging (CT scans, MRI, standard X-rays) and intra-operative visualization (ultrasound images) [1], [2], [3]. In many cases, real-time visual and sensory feedbacks are not available due to cost, accuracy and radiation exposure. Therefore haptic feeling of surgeons is very important in controlling the insertion operation. Fig. 1 shows an example of epidural injection procedure by inserting a catheter into the epidural space for anesthesia. It can be seen from the figure that catheter steering in order to avoid critical structures is needed.

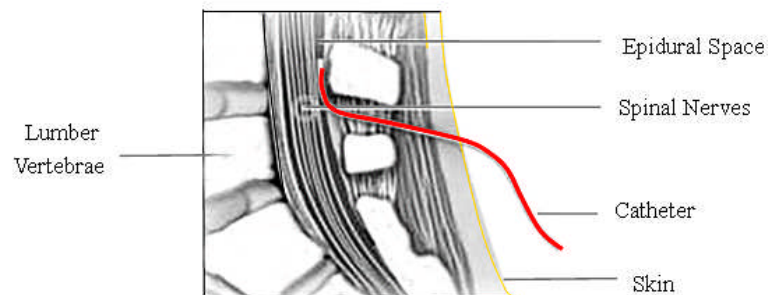


Fig. 1: A typical epidural injection procedure

When the needle moves in the complicated human tissues, a stable and steerable motion is crucial. Because the needle can deflect inside the tissue and the tissue can also deform, surgeons must predict the deflections and deformations [4].

The ability to curve around critical structures has become one of the major topics in needle or catheter insertion modeling.

Slight steering of symmetric-tip needles has been addressed in previous work by translating and orienting the needle base to cause tissue deformations that can guide the needle to avoid obstacles [5]. But for symmetric-tip needles, the capability of steering is limited because of the uniform force on needle tip. Some recent researches have explored ways of motion planning for flexible bevel-tip needle when moving inside soft tissues [6], [7], [8]. Resistant force caused by homogeneous (assumed) tissue acts on the asymmetric needle tip and makes the needle bend. Experiments have been done using series of different bevel angles, which affect the needle path a lot [9] [10]. The needle's turning curvature and moving path can also be controlled by changing the insertion speed and rotation angle [11], [12]. There is much uncertainty due to needle mechanics, tissue properties and interaction forces, so the following hypotheses have been made for path planning in previous works: very large needle torsional stiffness, stiff tissue properties, and nonholonomic motion with a steering constraint [7][8].

Our approach proposed in this paper differs significantly from previous needle steering works. A new compliant needle is designed to introduce a more effective way of needle steering with the aid of magnetic force. It has a larger turning curvature and better controllability even in deformable tissues. Some difficult targets in locations used to be inaccessible can now be reached using the compliant needle.

2. METHOD

2.1 Compliant Needle Modeling

The compliant needle is modified from the traditional symmetric-tip needle (shown in Fig. 2(a)) with the introduction of a compliant hinge as shown in Fig. 2(b). When needed, the compliant needle may have more than one compliant hinges.

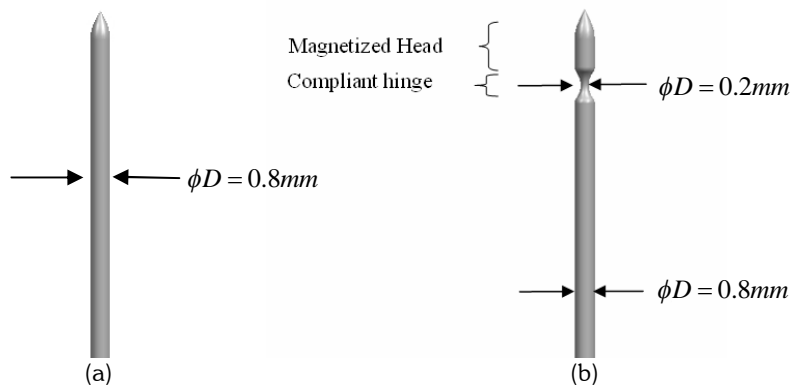


Fig. 2: Traditional needle and compliant needle.

The compliant needle has a weakened neck in the front near the tip, which is flexible enough to bend yet strong enough to withstand the load. The head of needle is magnetized, making it easier to act in the magnetic field. The rest of the needle is made of diamagnetic material that can not be affected by magnetic field. Fig. 3 shows the behavior comparison of a traditional needle and a compliant needle when applied the same force in finite element analysis software COSMOSWorks. Obviously the compliant needle has a larger turning angle than the traditional one, making it easier to turn when facing obstacles.

By controlling the magnitude and direction of magnetic force, the needle's moving direction can be switched, so as to bypass the critical structures such as nerves, arteries, blood-brain barrier, sensitive tissues and so on. This magnetic force aided steering has a great advantage in path control as it can turn the needle head in all directions in 3D space. Fig. 4 illustrates a path control method in which the white block represents a super strong rare earth magnet. By changing position and posture of the magnet, the reaction force between needle head and magnet can be adjusted. And the turning curvature of the needle can be large enough because the magnetic force is adjustable. Additionally, the turning stage can be carried out when the needle is in static state, which increases the accuracy. So the magnetic force

aided compliant needle steering method can largely minimize misplacement, reduces risks and give instant and optimal path planning.

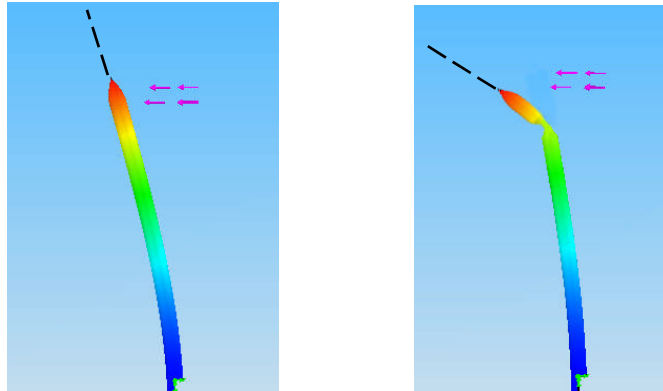


Fig. 3: Comparison of the needle deflection.

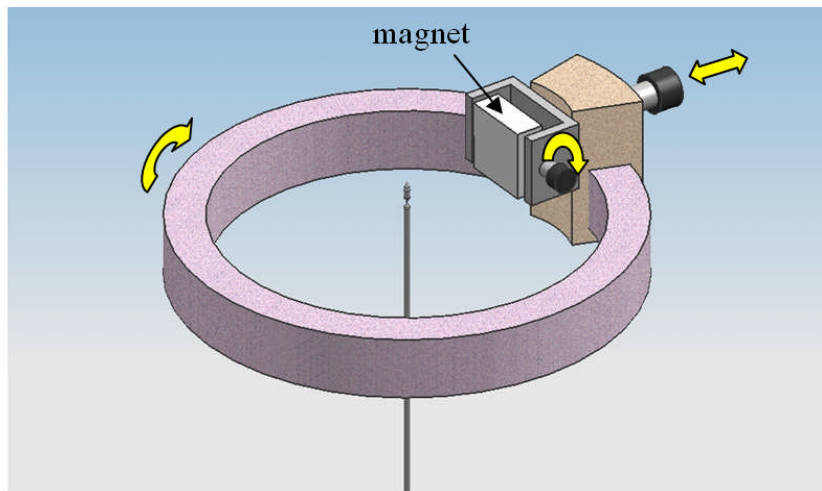


Fig. 4: The schematic of 3D needle steering.

2.2 Force Analysis

The magnetic force at the operating point P shown in Fig.5 is calculated based on reference [13] as:

$$F = \frac{B_g H_g}{2} \cdot A_g \quad (2.1)$$

where B_g is the gap flux density, H_g is the intensity of magnetic field in the gap, A_g is the air-gap area ($A_g = W \cdot L$).

And the relationship between flux density and intensity of magnetic field is:

$$B = \mu_0 \cdot (1 + X_m) \cdot H \quad (2.2)$$

where X_m is the magnetizing ability of the medium, μ_0 is a constant of proportionality.

The flux density at point P is:

$$B_{(P)} = \frac{B_r}{\pi} \left[\tan^{-1} \frac{LW}{2x\sqrt{L^2 + W^2 + 4x^2}} - \tan^{-1} \frac{LW}{2(x+T)\sqrt{L^2 + W^2 + 4(x+T)^2}} \right] \quad (2.3)$$

where B_r is the residual flux density decided by the material of the magnet.

According to Eqn. (2.1-2.3), the magnetic force acting on the needle head can be decided. Eqn. (2.3) is an empirical formula with a certain error compared with the practical result. Usually, it should be multiplied by a 0.8-0.9 correction factor. And Eqn. (2.1-2. 2) can be simplified as $F = \frac{B_{\theta}^2 A_{\theta}}{8\pi \times 10^{-7}}$ when using the SI units.

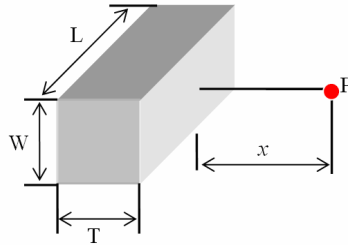


Fig. 5: Calculation of flux density at point P.

Bending of the needle head can be simplified as bending a rigid beam with a small-length flexural pivot as shown in Fig. 6(a). The rest of the needle after the flexural pivot can be considered as fixed because of the supporting force exerted by the tissue around it. The deflection can be ignored as it is small enough compared with the displacement of the needle head. Assuming the magnetic force is kept at the same angle ϕ with the needle head and the tissue is isotropic elastic with a spring constant μ which causes a non-uniform load when the needle head rotates, the turning angle can be derived according to the pseudo-rigid-body model as shown in Fig. 6(b).

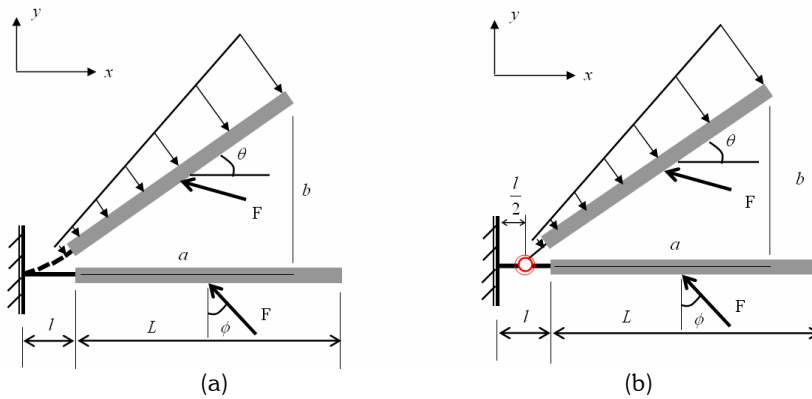


Fig. 6: Small-length flexural pivot and its pseudo-rigid-body model.

The moment caused by the elastic force of the tissue can be approximated as:

$$M_t = \frac{[\mu \cdot \theta \cdot (\frac{l}{2} + L)] \cdot [(\frac{l}{2} + L)]}{2} \cdot \frac{2}{3} (\frac{l}{2} + L) = \theta \cdot \frac{\mu}{3} \cdot (\frac{l}{2} + L)^3 \tag{2.4}$$

So the resultant moment of the system is:

$$T = F \cos \phi \cdot (\frac{L}{2} + \frac{l}{2}) - M_t \tag{2.5}$$

For the pseudo-rigid-body model, the equivalent torsion spring stiffness is $K = \frac{(EI)_l}{l}$, then

$$T = K \cdot \theta = \frac{(EI)_l}{l} \cdot \theta \tag{2.6}$$

Combining Eqn. (2.4-2.6), the turning angle can be obtained:

$$\theta = \frac{\frac{1}{2} F \cos \phi \cdot (L + l)}{\frac{(EI)_l}{l} + \frac{\mu}{3} \cdot \left(\frac{l}{2} + L\right)^3} \quad (2.7)$$

So the relationship between turning angle and flux density is:

$$B = \sqrt{\frac{8\pi \times 10^{-7} \cdot 2\theta \cdot \left[\frac{(EI)_l}{l} + \frac{\mu}{3} \left(\frac{l}{2} + L\right)^3\right]}{\cos \phi \cdot (L + l)}} \quad (2.8)$$

From Eqn. (2.8), the turning angle of a needle can be controlled by adjusting the value of flux density. For example, to turn the needle head 15 degree to 30 degree, the required magnetic field is $0.0391T - 0.0553T$ (if we set $l = 0.001m$, $L = 0.0035m$, the needle neck diameter $0.0002m$ and the area of magnet pole $0.05m \times 0.06m$).

The theoretical model described above can be used to predict the turning angle of needle and its moving path in the tissue. If more detailed physical properties of human tissue can be obtained, FEM analysis would be used. Fig. 7 illustrates the result of a FEM analysis by COSMOSWorks, in which the symbol URES (m) represents the resultant displacement. The figure shows an exploded view of a needle inserted into a homogeneous tissue under a magnetic force on its head. By controlling the magnitude and direction of the magnetic force, operators can steer the needle in a desired path. In the presence of different types of tissues, magnetic force should be adjusted from time to time to insure the accuracy.

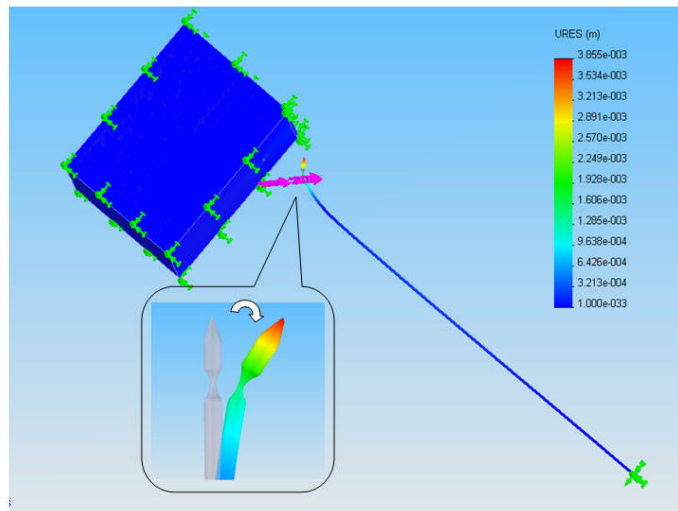


Fig. 7: FEM analysis of needle turning in the tissue.

3. STEERABLE NEEDLE INSERTION SIMULATION

3.1 Soft Tissue Modeling

In needle insertion, the surgeon's haptic feeling is very important in controlling the insertion. In simulating the needle insertion, setting the right tissue model is very important. Soft tissues have fundamentally different behavior due to the different biological constituents. As the needle penetrates the tissue, there would be tissue deformation, sliding and peeling, stick-slip friction between tissue and needle [14]. Due to the complex structure and physical phenomena, it is not possible to characterize their properties linearly. And linear models are not suitable for large deformations, which may result in "ghost force" and make elements artificially inflate. To solve this problem, Müller proposed a co-rotational FEM method by multiplying the stiffness matrix with element rotations of a local frame with respect to its initial orientation [15]. In our simulation program, to simulate the dynamic behavior of deformable tissue in real time, this co-rotational FEM method is employed to calculate the nodal force:

$$f_e = R_e K_e (R_e^{-1} x - x_0) = R_e K_e R_e^{-1} x - R_e K_e x_0 = K'_e x + f_{e0} \quad (3.1)$$

where R_e is a 12×12 matrix that contains four copies of the 3×3 rotation matrix along its diagonal, K'_e is the element's rotated stiffness matrices, and f_{e0} is the force offsets.

3.2 Force Modeling

An energy-based fracture mechanics approach [16] is used to model the force which will be sent to the user through our haptic interface. The reaction force F_h for haptic rendering is calculated as:

$$F_h = -F_t = -\left(\frac{\Delta U}{\Delta x} + \frac{2\pi J_c r \Delta l}{\Delta x}\right) \tag{3.2}$$

where ΔU is the change of elastic potential energy which can be calculated by FEM, J_c is the fracture toughness which represents the work required to propagate a crack of unit of area inside a body, Δl is the increase of insertion depth, r is the needle radius, Δx is the displacement of the haptic device.

The entire procedure of needle insertion can be considered as two stages: deformation and penetration. If the exerted force F_t on the tissue is smaller than the tissue rupture force (this parameter is set according to experimental results of tissue properties), the tissue will only deform and won't be penetrated as shown in Fig. 8(a). Otherwise, deformation and penetration can be observed at the same time, as shown in Fig. 8(b).

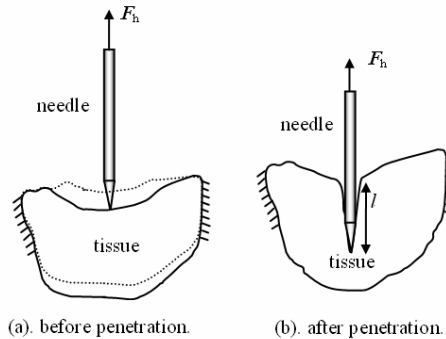
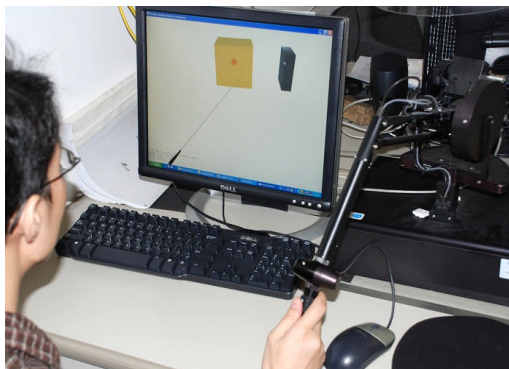


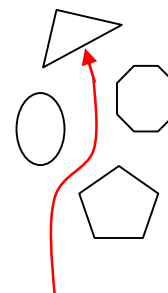
Fig. 8: Needle insertion stages.

3.3 Needle Steering Simulation

A Phantom® Premium 1.5/6-DOF device is used for the haptic simulation, as shown in Fig. 9(a). By moving the handle of the haptic device in a 3D space, user can control the virtual needle to penetrate the tissue and have a real time visual and haptic feedback. Fig. 9(b) shows a typical obstacle avoidance task in needle insertion. The triangle represents a target. In order to reach the target, obstacle avoidance is necessary. The turning of the needle head is controlled by moving the magnetic block and the thrusting of the needle is controlled by the haptic device. Homogeneous soft tissue and force modeling methods introduced above are used in the haptic rendering process of the simulation.



(a)



(b)

Fig. 9: Needle insertion simulation.

Fig. 10 illustrates the magnetic force aided needle steering when a needle is being inserted. Before the needle penetrates the tissue, there is a deformation on the tissue, as shown in Fig. 10(a). After penetration, as the needle moves inside the tissue and to the magnetic field, the magnetic force causes the needle head to turn, as shown in Fig. 10(b). When moving and rotating the magnet shown as a cuboid in Fig. 10(c) and Fig. 10(d), the magnetic force guides the needle to curve around the obstacle located at the center of the tissue. This would be very useful in the path planning process. Users can also set different values of the magnetic force, which cause different turning curvatures. The process is easy to control with a real time visual and haptic feedback.

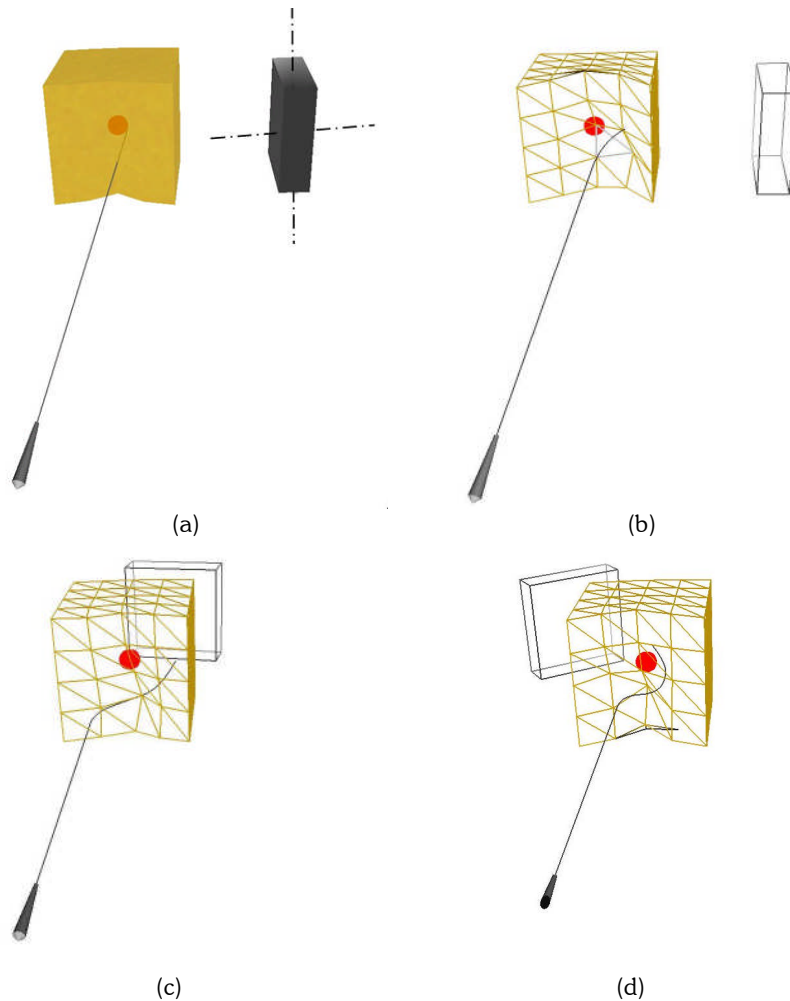


Fig. 10: Steerable needle insertion simulation.

4. CONCLUSIONS

A compliant needle is designed from the conventional symmetric-tip needle, making it easier to steer. Magnetic force is used to aid the path control of the brand-new compliant needle. This compliant needle steering method has its advantages in large turning curvature and path controllability. The steerable needle insertion process is simulated and implemented in a haptic system to give the user both visual and haptic feedback.

Future work will be focused on exploring more complicated nature of needle steering in heterogeneous tissues.

Experiments for needle insertion in phantom tissues with heterogeneous properties under adjustable magnetic force are being designed.

5. REFERENCES

- [1] Hata, N.; Dohi, T.; Warfield, S. K.; Wells, III, W. M.; Kikinis, R.; Jolesz, F. A.: Multimodality Deformable Registration of Pre- and Intraoperative Images for MRI-Guided Brain Surgery, *Proceedings of MICCAI '98*, Springer-Verlag Lecture Notes in Computer Science, 1492, 1998, 1067-1074.
- [2] Wagner, C. R.; Perrin, D. P.; Howe, R. D.; Vasilyev, Nikolay; del Nido, P. J.: Force Feedback in a Three-Dimensional Ultrasound-Guided Surgical Task, *Proceedings of the IEEE Virtual Reality Conference*, 2006, 5.
- [3] Alterovitz, R.; Branicky, M.; Goldberg, K.: Constant-Curvature Motion Planning Under Uncertainty with Applications in Image-Guided Medical Needle Steering, in *Proc. Workshop on the Algorithmic Foundations of Robotics*, Jul. 2006.
- [4] Kataoka, H.; Washio, T.; Chinzei, K.; Mizuhara, K.; Simone, C.; Okamura, A. M.: Measurement of the Tip and Friction Force Acting on a Needle during Penetration, *Proceedings of the 5th International Conference on Medical Image Computing and Computer-Assisted Intervention*, 2002, 216 - 223.
- [5] Heverly, M.; Dupont, P.; Triedman, J.: Trajectory Optimization for dynamic Needle Insertion, *International Conference on Robotics and Automation*, 2005, 1646-1651.
- [6] Alterovitz, R.; Goldberg, K.; Okamura, A.: Planning for Steerable Bevel-tip Needle Insertion Through 2D Soft Tissue with Obstacles, *IEEE International Conference on Robotics and Automation*, 2005, 1652-1657.
- [7] Webster, III, R. J.; Kim, J. S.; Cowan, N. J.; Chirikjian, G. S.; Okamura, A. M.: Nonholonomic Modeling of Needle Steering, *International Journal of Robotics Research*, 25(5-6), 2006, 509-525.
- [8] Park, W.; Kim, J. S.; Zhou, Y.; Cowan, N. J.; Okamura, A. M.; Chirikjian, G. S.: Diffusion-Based Motion Planning for a Nonholonomic Flexible Needle Model, *IEEE International Conference on Robotics and Automation*, 2005, 4611-4616.
- [9] O'Leary, M. D.; Simone, C.; Washio, T.; Yoshinaka, K.; Okamura, A. M.: Robotic Needle Insertion Effects of Friction and Needle Geometry, *Proceedings of the 2003 International Conference on Robotics & Automation*, 2003, 1174-1180.
- [10] Webster, III, R. J.; Memisevic, J.; Okamura, A. M.: Design Considerations for Robotic Needle Steering, *Proceedings of the 2005 IEEE International Conference on Robotics and Automation*, 2005, 3588-3594.
- [11] Engh, J. A.; Podnar, G.; Khoo, S. Y.; Riviere, C. N.: Flexible Needle Steering for Percutaneous Navigation within Deep Zones of the Brain, *Bioengineering Conference*, *Proceedings of the IEEE 32nd Annual Northeast*, 2006, 103-104.
- [12] Alterovitz, R.; Lim, A.; Goldberg, K.; Gregory, S.; Chirikjian; Okamura, A. M.: Steering Flexible Needles Under Markov Motion Uncertainty, *Proc. IEEE/RSJ International Conference on Intelligent Robots and Systems (IROS)*, 2005, 120-125.
- [13] Campbell, P.: *Permanent Magnet Materials and their Application*, Cambridge University Press, 1996, 8, 104
- [14] Brett, P. N.; Parker, T. J.; Harrison, A. J.; Thomas, T. A.; Carr, A.: Simulation of resistance forces acting on surgical needles, *Proceedings of the Institution of Mechanical Engineers, Part H, Journal of Engineering in Medicine*, 211, 1997, 335-347.
- [15] Müller, M.; Dorsey, J.; McMillan, L.; Jagnow, R.; Cutler, B.: Stable real-time deformations, *Proceedings of ACM SIGGRAPH Symposium on Computer Animation*, 2002, 49-54.
- [16] Mahvash, M.; Hayward, V.: Haptic Rendering of Cutting: A Fracture Mechanics Approach, *Haptics-e, The Electronic J. Haptics Research*, 2(3), 2001